PCCP

Accepted Manuscript

ROYAL SOCIETY OF CHEMISTRY

www.rsc.org/pccp

PCCP

RSCPublishing

ARTICLE

Relativistic DFT calculations of magnetic moments on pristine and thiolated Mn@Au$_x$ (x = 6, 12)

Cite this: DOI: 10.1039/x0xx00000x

G. Raggi,[a*] and J. R. Soto[b],

Received 00th January 2012,
Accepted 00th January 2012

DOI: 10.1039/x0xx00000x

www.rsc.org/

In this work we present results from relativistic DFT calculations of magnetic moments for manganese inserted into a gold ring (Mn@Au$_6$) or cage-like structure (Mn@Au$_{12}$) both pristine and n-thiolated. Optimization has been carried out to obtain different isomers always favouring the endohedral gold clusters with the Mn inside. For the total magnetic moment (from electronic population analysis) a verification of the jellium model has been performed in each case. It is concluded that the magnetic moments arise largely from the doped manganese atom and that thiolation can modulate its value, which is not present in the pure form. In the Mn@Au$_{12}$ clusters we observed the formation of a hole, in their structure; this could be a characteristic of insertion of a highly ferromagnetic dopant in some metal clusters, such as gold, and these could act as a precursor of the formation of gold magnetic nanotubes.

I. Introduction

Gold has unique properties; it is a heavy element and its electronic structure has important relativistic effects[1–7]. The clusters formed by gold are characterized as having a large number of stable isomers planar or three-dimensional, with lower or higher symmetry, leading to different magnetic moments. The magnetic moments of gold clusters depends on the structure and number of atoms[8–11]. For example, the most stable isomer for Au_7, has C_S symmetry, a binding energy (E_b) of 1.8 eV and HOMO-LUMO gap (HL-gap) of 1.077 eV. [9,10,12]. Some of these isomers have been fully characterized experimentally and theoretically using techniques like far infrared multiple-photon dissociation (FIR-MPD) on clusters produced by laser vaporization[10,12–14].

When a gold cluster is doped with transition metals it is possible to obtain physical and chemical properties for potential applications in: optics, solid state physics, microelectronics, nanotechnology, biology and other areas[8,9,15,16]. Some experimental and theoretical work has shown that the introduction of a dopant atom in metallic clusters can drastically change their properties[15–19]. Specifically introducing a Mn atom inside a gold cluster can not only increase the stability[12] but also affects the magnetic properties[12,20–26]. Experimental evidence for changing magnetic properties in Mn and Au clusters has been found by Schiller[21], also M. Zhang *et al*[15] have reported for the Mn@Au$_6$ cluster with D_{6h} symmetry a magnetic moment of 3.0 μ_B is present; in addition, they also calculated a HL-gap of 0.72 eV. and a E_b of 2.35 eV. In general, gold clusters doped with manganese have been observed to exhibit enhanced magnetic properties up to ultrahigh values of 44.0 μ_B in Mn_{13}@Au_{20} with octahedral symmetry[24]. Janssens *et al*[17] established the stability of cationic gold clusters doped with Mn by employing mass spectrometric analysis of fragments resulting from intense irradiation of a cluster beam. The enhanced stability of the fragments led to the first observation of 2D magic numbers, consistent with a square well potential with triangular, circular and square symmetries. The first seven magic numbers observed by this group, for example, with circular symmetry are 2, 6, 10, 12, 16, 20 and 24.

Using protecting ligands like methanothiolates (SCH_3) in nanoparticles, such as gold, makes a film relatively inert against external agents, providing enhanced stability, well defined monodispersity for potential applications in nanotechnology, biology, catalysis, spintronics, photophysical and magneto-physical devices[27–31]. Synthesis and isolation of self-assembled thiolate clusters has been conducted successfully over the past decade[32–37]. Iwasa *et al*[28] reported a variable magnetic moment in gold with thiolates $[Au_{25}(SCH_3)_{18}]^n$ for n = 3-, 2-, 1-, 0, 1+, 3+.

In the present work we report results of relativistic DFT calculations of the structure, stability, total magnetic moment and spin density of nanostructures composed by endohedral Mn@Au$_6$ and Mn@Au$_{12}$ clusters, in both their pure and n-thiolated forms. The number of thiolates added to the metallic structure might be used to modulate the magnetic moments of the clusters.

II Methodology

For the present work calculations have been carried out using the Amsterdam Density Functional (ADF) code[38] based on Density Functional Theory (DFT)[39]. The exchange-correlation functional used is the generalized gradient approximation of Perdew and Wang (GGA-PW91)[40] which has previously been shown to be accurate for transition metals[15]. All calculation were performed with relativistic scalar zeroth-order regular approximation (ZORA) into Dirac equation for the relativistic effects[38,41]. The optimization process used a quasi-Newton approach with the BFGS-Hessian matrix updated formula. Since ADF employ Slater-type functions for the basis set, all the final calculations are all-electron and of quadruple-*zeta* plus four polarization functions (QZ4P)[38] quality. We used Mulliken population analysis[42] (MPA) and multipole derived charge analysis (MDC)[43] to estimate the average spin density in order to determinate the contribution of the Mn to the total magnetic moment. It is convenient to outline the method we employ to determine the multiplicity (M) for the lowest-lying isomer. We performed geometry optimizations varying in every case the M from the lowest possible to the likely highest: a singlet state followed by triplet, quintuplet, etc state; or double, quadruple, sextuple state. In each case, we selected the multiplicity with the lowest binding energy and we performed vibrational frequencies analyses to probe the isomer stability. In cases which gave all real frequencies, relative binding energies were computed with respect to the lowest energy.

III Results and discussion

In the first instance we optimized the structure for some $Mn@Au_6$ isomers previously reported in refs. 12 and 15 using PW91 and PW91/BP86 exchange-correlation functionals respectively. In Table 1 the results for the three low lying stable isomers are shown, including their point group symmetry, M, total magnetic moment, magnetic moment of the Mn atom, relative binding energy (BE) and HL-gap. The optimized skeletal structures for these isomers are shown in Fig. 1 including the bond lengths. For the two first isomers (of C_s and D_{6h} symmetry) we obtain good agreement with Dong *et al*[12], but with a BE of 0.07 eV against 0.13 eV; while the results from Zhang *et al*[15] are in reverse order compared to ours, and have a large BE difference (1.83 eV); these big differences are perhaps due to another spin multiplicity being considered for the C_s isomer (the total spin was not reported in ref. 15). The bond lengths of the C_S isomer compared with that reported in 12 have a maximum difference of 0.1 Å and its HL-gap is approximately 1.0 eV, which is in agreement with ref. 12. The HL-gap of the D_{6h} structure is 0.7 eV and is in excellent with that reported in ref. 15 (0.72 eV). With respect to the third isomer we found it had C_{2v} symmetry rather than C_{3v} has reported by Dong *et al*[12]. Regarding the magnetic moments in the Manganese atom for the D_{6h} isomer, we report 3.68 vs 4.28 μ_B[15] and for C_s ,4.13 vs 4.56 μ_B[12]. These differences may be due to the inclusion of the relativistic effects using ZORA giving a better description of the spin density for the diffuse gold valence electrons.

	Our results			Dong *et al*[12]		
	C_s	D_{6h}	C_{2v}	C_s	D_{6h}	C_{2v}
M	6	4	6	6	4	6
$\mu(\mu_B)$	5	3	5	-	-	-
μ_{Mn} (μ_B)	4.13	3.68	4.44	-	-	-
BE (eV)	0.00	0.07	0.49	0.00	0.13	0.27
HL-Gap (eV)	1.03	0.70	0.29	-	-	-

Table 1 Low-lying stable isomers of Au_6Mn as compared with Dong *et al*[12] isomers for Multiplicity (M), total magnetic moment μ $[\mu_B]$, magnetic moment of Mn (μ_{Mn}) (MPA), Binding Energy (BE) and HUMO-LUMO gap.

We can explain directly the resulting total magnetic moment in D_{6h} isomer using the phenomenological shell model (PSM) or jellium model for metallic clusters, in which 2 of the 5 unpaired electrons in the Mn are paired with the Au_6 ring valence electrons leaving unpaired electrons in the d_{yz}, d_{xz} and d_{z2} orbitals, giving a magnetic moment of 3.0 μ_B[22]. To verify if this is in agreement with the jellium model, we have 6 unpaired electrons from the 6 gold atoms ($\ldots 6s^1$) and 7 from the manganese ($\ldots 4s^2 3d^5$) giving a total of 13. The corresponding magic number for a circular symmetry structure is 10 (see ref. 17) and there are 3 unpaired electrons, giving a magnetic moment of 3.0 μ_B. For the C_S symmetry, which is the most stable, there is a drastic decrease in planar symmetry and so the magic number also decreases; in this case it is 8 with a square well potential with a triangular symmetry[17] giving a magnetic moment of 5.0 μ_B. Two Mn electrons are transferred to the triangle forming the apex opposite to Mn (see Fig. 1a). The C_{2V} symmetry structure fits better in a square well potential with square symmetry[17], so the magic number corresponds also to 8 and the resulting magnetic moment is 5.0 μ_B. The Mn transfers only two electrons to the four gold atom of the isomer basis of Fig. 1c.

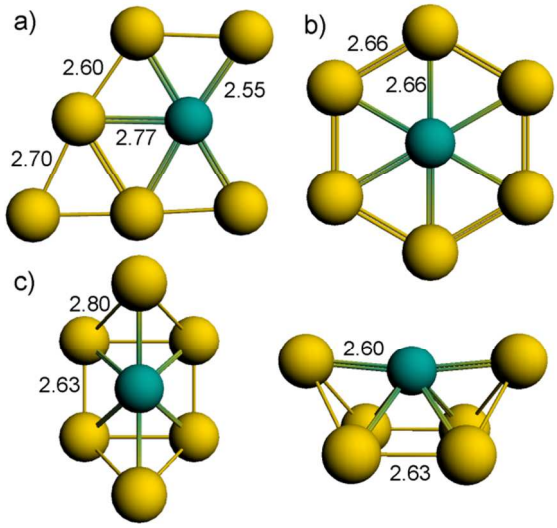

Fig. 1. Cluster of $Mn@Au_6$ in three different symmetries a) C_s, b) D_{6h} and c) C_{2v} (two views).

$Mn@Au_6SCH_x$ (*X=1,2,…,6*)

Iwasa *et al*[28] found tunable magnetic moments in charged thiolated core-in-cage gold clusters, however, we will see in the present work by selecting the number of thiolates we can modulate the magnetic moments in neutral endohedral Mn in a gold ring or gold cage clusters. To see how the molecular orbitals are filled in the cluster according to the jellium model (considering the thiolate influence as a small perturbation), the sulphur in the thiolates must be considered as a donor of one electron to the molecular orbitals (MO). The six gold atoms in the ring are treated similarly, which provides 6 electrons to the cluster, one per gold atom ($\ldots 6s^1$). Finally, for the manganese atom we have 7 electrons ($\ldots 4s^2 3d^5$). In Table 2 we tabulate the total bond energy (E_b), the binding energy per thiolate ($E_{b/t}$) calculated from eq. 1, the total magnetization μ, multiplicity, HL-gap and the valence electron distribution according to the jellium model. For the $E_{b/t}$ we used the values $E_b[Mn@Au_6]$ = -21.16 eV and $E_b[SCH_3]$ = -22.70 eV and these represent the binding energy per thiolate between the hexagonal gold ring and the thiolates. For the single-thiolated complex (Fig. 2a), the lowest-lying structure is with the thiolate on bridge and we have a total of 14 valence electrons which include one electron from the S, 6 electrons from the Au ring, and 7 electrons from Mn. The magic number is 10 in this case, one from S, 6 from Au and 3 from Mn, with the remaining 4 electrons unpaired, giving us a total magnetic moment of 4.0 μ_B (see Table 2).

$$\frac{E_b}{t}\left[Mn@Au_y(SCH_3)_x\right] = \left(E\left[Mn@Au_y(SCH_3)_x\right] - E\left[Mn@Au_y\right] - x(E[SCH_3])\right)/x \quad (1)$$

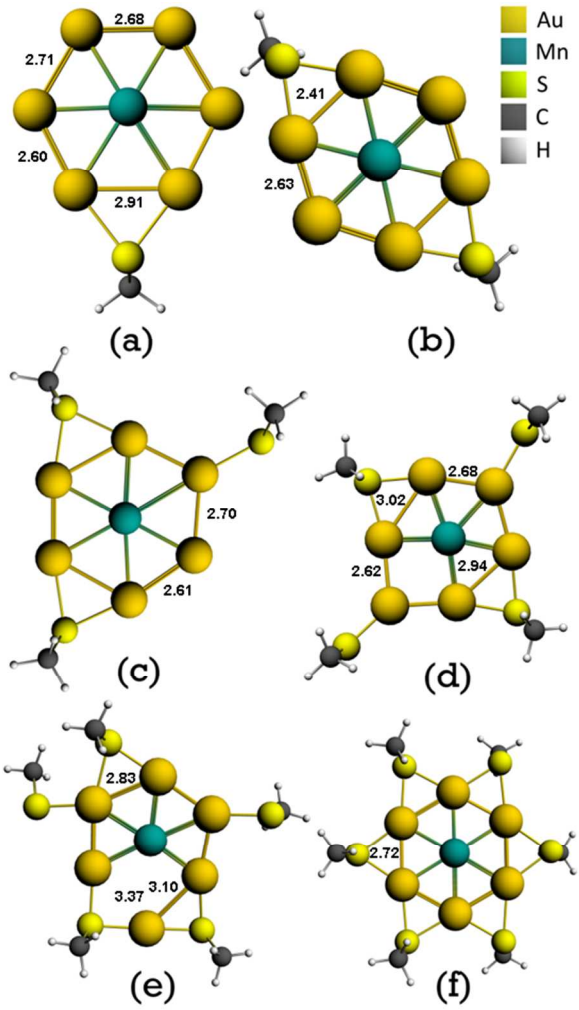

Fig. 2. Equilibrium ground state isomers for $Mn@Au_6$ + (a) 1 thiolate, (b) 2 thiolates, (c) 3 thiolates, (d) 4 thiolates, (e) 5 thiolates and (f) 6 thiolates.

	D_{6h} – Hexagonal					
	E_b (eV)	$E_{b/t}$ (eV)	μ [μ_B]	M	GAP HL	"jellium"
$Mn@Au_6SCH_3$	-47.09	-3.23	4	5	0.7	1e_S + 6e_Au + 3e_Mn = 10e
$Mn@Au_6[SCH_3]_2$	-71.42	-2.43	3	4	0.31	2e_S + 6e_Au + 4e_Mn = 12e
$Mn@Au_6[SCH_3]_3$	-97.07	-2.60	4	5	0.56	3e_S + 6e_Au + 3e_Mn = 12e
$Mn@Au_6[SCH_3]_4$	-121.47	-2.38	5	6	0.76	4e_S + 6e_Au + 2e_Mn = 12e
$Mn@Au_6[SCH_3]_5$	-146.44	-2.36	4	5	0.42	5e_S + 6e_Au + 3e_Mn = 14e
$Mn@[AuSCH_3]_6$	-172.21	-2.48	5	6	0.89	6e_S + 6e_Au + 2e_Mn = 14e

Table 2 Total bond energy (from ec. 1 with *x=0* to 6 and *y=6*), average bond energy per thiolate, magnetic moment, spin multiplicity, HOMO-LUMO gap and electronic configuration in jellium model.

When another thiolate is added, the ring structure ($Mn@Au_6$) seems to be unaffected, conserving the internal symmetry (Fig. 2b). The low-lying arrange is with the two thiolates on bridge at opposite sides. The $E_{b/t}$ reduces by 0.8 eV indicating a lower binding of the thiolates to the hexagonal gold ring and is the only thiolated complex for which the total magnetic moment is the same as the bare cluster. The magic number for this cluster is 12, with the remaining 3 electrons being unpaired, which implies a magnetic moment of 3.0 μ_B. The HL-gap decreases significantly with respect to the one thiolate cluster by 0.39 eV. The magnetic moment, according to the jellium model, with three thiolates (two on bridge and one on top alternating see Fig. 2c), ($Mn@Au_6(SCH_3)_3$) means the manganese atom gives 3 electrons to the cluster, the sulphur atoms give 3, and the gold atoms 6, with the remaining 4 electrons unpaired. The HL-gap increases slightly with respect to 2-thiolated cluster, by 0.25 eV and also the $E_{b/t}$ by 0.17 eV. The $Mn@Au_6[SCH_3]_4$ cluster (two thiolates on bridge, two on top in opposites sides) shows an increase in the HL-gap of 0.76 eV and the magnetic moment becomes 5.0 μ_B. In this case, the isomer has some distortion in the Au ring plane bending opposite to the direction of the thiolates orientation (Fig. 2d); however, the jellium model, when applied to the cluster with circular symmetry gives a magic number of 12 (Table 2) and 5 unpaired electrons. For the cluster with 5 thiolates the central hexagonal symmetry breaks as well, and two thiolates align with the gold ring breaking the symmetry (Fig. 2e). The contribution to the magnetic moment comes from: 5 electrons from S atoms, 6 from the Au ring and 3 from manganese. Since the symmetry is broken, we find 14 paired electrons on the gold ring (non magic number) and 4 electrons unpaired on the Mn atom, and so the magnetic moment is 4.0 μ_B. Finally, for the cluster with 6 thiolates (all thiolates on bridge, see Fig. 2f) the central ring appears to have hexagonal symmetry D_{6h}, however, given the different orientation of the C atoms the symmetry reduces to C_2, and so the number of paired electrons were found to be 14, leading to a magnetic moment of 5.0 μ_B. The structure with this symmetry has three thiolates pointing down from the principal axis of the central gold ring and three pointing up, distributed uniformly, with each sulphur forming two single bonds with two gold atoms. According to Table 2, this cluster has the biggest chemical stability with 0.89 eV. $E_{b/t}$ has an average value of 2.45 for all the n-thiolated complexes with $2 \leq n \leq 6$.

Table 3 shows the spin density for the principal elements of the cluster: gold, manganese and thiolates taken from MPA[42] where the Mn atom seems to be the principal contributor to the total magnetic moment. The thiolates by themselves do not play a significant role in the magnetic moment, except for $Mn@Au_6(SCH_3)_2$, there seems to be an incremental tendency in the total magnetic moment with an even/odd alternation.

	Number of Thiolates						
	0	1	2	3	4	5	6
Au	-0.68	0.22	-0.36	0.48	0.79	0.33	0.79
Mn	3.68	3.83	3.83	3.81	4.03	3.93	4.11
SCH_3	---	-0.06	-0.46	-0.29	0.18	-0.25	0.09
Sum	3.00	4.00	3.00	4.00	5.00	4.00	5.00

Table 3 Spin density contribution (from MPA) of Au_6, Mn and SCH_3 to the total magnetic moment of the clusters with 0 to 6 thiolates in Bohr magnetons [μ_B].

$Mn@Au_{12}$

The cluster $Mn@Au_{12}$ becomes a cage-like structure of gold for all symmetries, with the manganese atom approximately in the centre of mass of the gold atoms. The first isomeric symmetry we tried to stabilize was of I_h (Fig. 3a) for which we obtained a converged geometry for each of the doublet, quadruplet, and sextuplet states, but each of these has at least one imaginary frequency, meaning the icosahedral isomer is not stable. In Table 4 are tabulated the binding energies, HL-gap, spin-density on gold and Mn, total magnetic moment and M for the $Mn@Au_{12}$ isomers showed in Fig. 3. All the isomers have similar binding energies however the HL-gap of I_h is notably lower confirming its instability. Both isomers D_{6h} and C_s are

not denoted by their point symmetry group but their initial symmetry before optimization.

$Mn@Au_{12}$	BE (eV)	GAP HL	SD-Au	SD-Mn	μ [μ_B]	M
O_h	-36.75	0.36	1.07	3.93	5	6
D_{6h}^{+}	-36.70	0.39	-0.73	3.73	3	4
I_h*	-36.37	0.08	-2.90	3.90	1	2
C_s^{+}	-36.03	0.18	0.95	4.05	5	6

Table 4 Bond energies, HL gap, Spin density of gold atoms, spin density of manganese (from MPA), magnetic moments and multiplicity for doped gold clusters with manganese.
[+] $2C_S$ and $2D_{6h}$ do not represent the symmetry, but only a way to identify structure following geometry optimization.
[*] not in equilibrium.

According to the spin density, the Mn is providing four unpaired valence electrons to the total magnetic moment of the cluster in each case, and the contribution of the gold atoms varies with the different symmetries. In the case of octahedral symmetry O_h (Fig. 3b), the gold atoms provide one electron and the Mn four, so we can write in terms of magnetic moments or spin density $Mn^{[+4]\mu_\beta}@Au_{12}^{[+1]\mu_\beta}$. This symmetry has the highest binding energy and a high HL-gap with respect the same group. This equilibrium symmetry was obtained breaking the icosahedral symmetry (I_h) using a thiolate attached to one of the gold atoms and allowing relaxation (see Fig. 4a), then removing the thiolate (Fig. 3b).

For the C_s symmetry also we obtain the magnetic moment distribution $Mn^{[+4]\mu_\beta}@Au_{12}^{[+1]\mu_\beta}$. This symmetry was obtained taking a structure of C_S symmetry (Fig. 1c) above another equal in parallel (in a sandwich) at certain distance from each other, and then allowed them to relax. This isomer competes in binding energy with O_h but has a lower HL-gap. The last of the equilibrium geometries, with a magnetic moment decomposition $Mn^{[+4]\mu_\beta}@Au_{12}^{[-1]\mu_\beta}$, was initiated with one D_{6h} structure above another like the C_S case; however this geometry lost symmetry when it was allowed to relax, but the binding energy difference is only 0.05 eV with respect to the D_{6h} structure. In this case the gold atoms have an opposite contribution to the total magnetic moment.

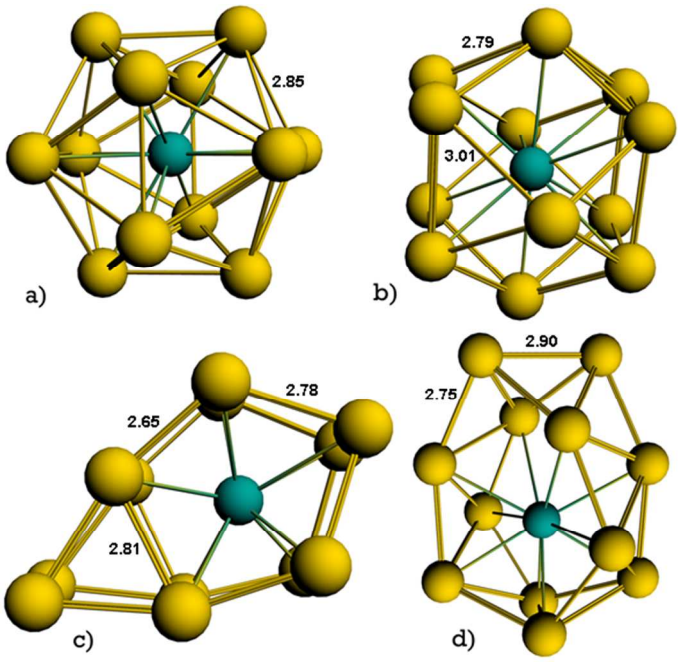

Fig. 3 Equilibrium geometries for pristine $Mn@Au_{12}$ in symmetries a) Icosahedral I_h, b) Octahedral O_h, c) Two C_S (one below the other) and d) two quasi hexagonal D_{6h} symmetry (one below the other) optimized with PW91 (ADF).

$Mn@Au_{12}SCH_x$ (*X=1,2,…,6*)

One of the methods used to obtain the octahedral symmetry was breaking the icosahedral symmetry through the adsorption of one thiolate to two gold atoms forming a bridge. The resulting complex is shown in Fig. 4a. The total magnetic moment of the octahedral structure decreased from 5 μ_B without the thiolates to 4 μ_B with one thiolate (see table 4); this may be because the sulphur atom donated one of its electrons to be paired with one of the unpaired gold electrons. In Table 4 are shown the binding energy, binding energy per thiolate, HL-gap, spin density per fragment and the total magnetic moment for the thiolated cluster as a function of the number of thiolates. The structure $Mn^{[+4]\mu_\beta}@Au_{12}^{[-1]\mu_\beta}(SCH_3)_2$ (Fig, 4e) comes from relaxation of an icosahedral structure with two thiolates at the sides, giving us two pentagons, one over the other, with two gold atoms displaced towards the thiolates. Looking at the cluster from above there is a hole seen where the only particle is the manganese atom exactly in the middle. The contribution of spin density (SD) of gold atoms to the μ_m is negative and compensated by the thiolates giving a total μ_m of 3 μ_B.

	E_b (eV)	$E_{b/a}$(eV)	HL-gap	SD-$(SCH_3)_x$	SD-Au	SD-Mn	μ_m [μ_B]
$Mn@Au_{12}SCH_3$	-62.321	-2.87	0.374	0.000	0.046	3.955	4
$Mn@Au_{12}[SCH_3]_2$	-86.340	-2.10	0.343	0.157	-0.670	3.513	3
$Mn@Au_{12}[SCH_3]_3$	-112.827	-2.66	0.386	0.011	0.826	3.163	4
$Mn@Au_{12}[SCH_3]_4$	-136.424	-2.22	0.070	0.329	-0.064	4.735	5
$Mn@[AuSCH_3]_{12}$*	-333.481	-2.03	0.038	0.310	0.122	4.569	5

Table 5 Bond energies, Bond energies by atom, HL gap, spin density of thiolats, spin density of golds, spin density of manganese (from MPA) and magnetic moment for thiolate doped gold clusters with manganese. (*we were unable to perform frequencies due to the cost of quantum chemical calculations).

Adding three thiolates to a I_h symmetry structure we found the structure $Mn^{[+3]\mu_\beta}@Au_{12}^{[+1]\mu_\beta}(SCH_3)_3$ (Fig. 4b). Only with the adsorption of up to three thiolates do we obtain chemical stability with HL-gaps of 0.37 eV on average from 4 thiolates onwards the isomers are not very stable (cases for more than 5 thiolates was not possible check stability through a Hessian calculation due to the huge demand of calculations). We show the 4 and 12 thiolated clusters only for comparison. In all cases the binding energy per thiolate is similar in average to the $Mn@Au_6$ thiolated cluster (2.26 eV) discounting one of single thiolated cluster energy which is significantly higher. The Fig. 4c shows us a geometry $Mn^{[+5]\mu_\beta}@Au_{12}^{0}(SCH_3)_4$ without any symmetry like the others, this comes from breaking the I_h symmetry with the thiolates. In this particular case the contribution to the $\boldsymbol{\mu_m}$ comes from the Mn atom. The same magnetic behaviour occurs with the 12-thiolated cluster $Mn^{[+5]\mu_\beta}@Au_{12}^{0}(SCH_3)_{12}$ (Fig. 4d). This symmetry exhibits, like the others, a clear hole with the Mn atom in the centre. The formation of these holes takes the form of cylindrical nanostructures with the addition of thiolates that resembles gold nanotubes[44].

Fig. 5 and 6 show the Mn contribution to the total magnetic moment of the bare and thiolated clusters. The contribution according to MPA of the Mn to the total magnetic moment of the n-thiolated $Mn@Au_6$ cluster has small variation for changing n in concordance to the internal structure (gold ring) which has small variations as well; however for 0 and 2 thiolates the Mn contribution is slightly above the total magnetic moment (see Table 3) implying opposite contributions of gold atoms and thiolates. The MDC-monopolar and dipolar do not have this excess of spin density contribution of Mn, but the MDC-quadrupolar gives a significant increase of the Mn magnetic moment for 0-2 thiolates implying a lower magnetic shielding of μ_{Mn} at short distances. For 3-6 thiolates the two charges partitioning schemes show similar trends with MDC 0.9 μ_B above MPA in average. In the n-thiolated $Mn@Au_{12}$ case the MPA-μ_{Mn} has important variations from 3.16 μ_B with three thiolates to 4.74μ_B with four thiolates according with drastic changes on the gold cage structure dependant on the number of thiolates. The MDC-μ_{Mn} shows a odd-even trend with μ_{Mn} always lower to 3 μ_B except for the 12-thiolates MPA-monopolar with a higher value of 4.60 μ_B. In general, the predicted MDC Mn contributions to the total magnetic moment of the clusters are lower than MPA and the MDC-m,d 2-thiolates and MDC-d,q 4-thiolates have values lower than 1.0 μ_B showing a great magnetic shielding effect for these thiolated gold cages according to this charge partitioning scheme.

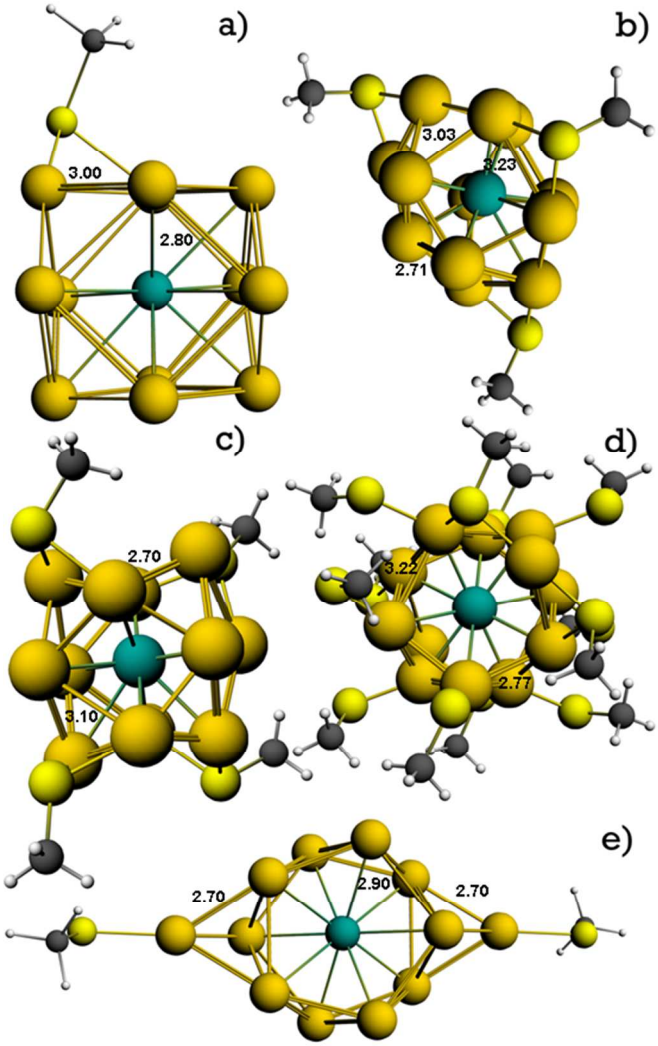

Fig. 4 Equilibrium geometries for thiolate $Mn@Au_{12}$ a) 1 thiolate (Octahedral O_h), b) 3 thiolates, c) 4 thiolates d) 12 thiolates and e) 2 thiolates optimized with PW91 (ADF).

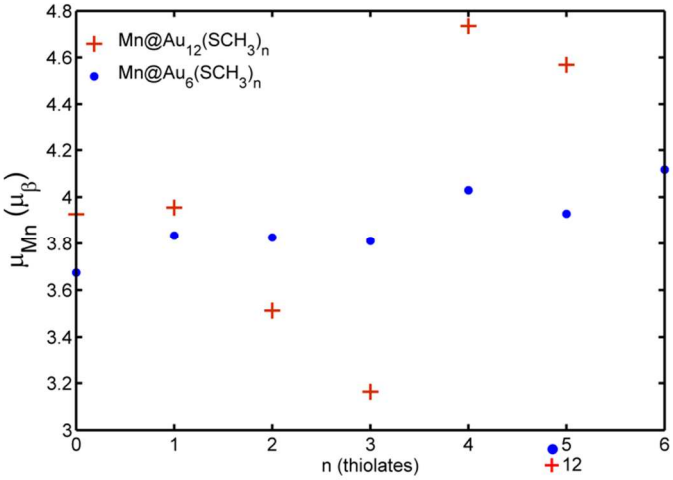

Fig. 5 Mn contribution (from MPA) to the magnetic moment to the cluster $Mn@Au_x(SCH_3)_n$ ($x=6$ in blue and $x=12$ in red) in Bohr magnetons, where n is the number of thiolates.

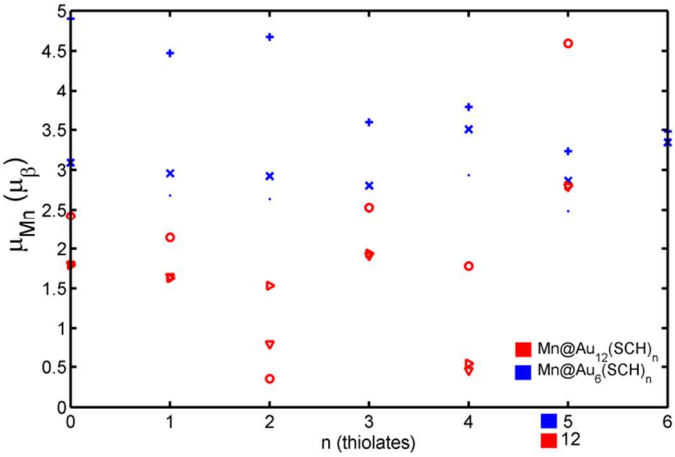

Fig. 6 Mn contribution to the magnetic moment to the cluster $Mn@Au_x(SCH_3)_n$ ($x=6$ in blue and $x=12$ in red) in Bohr magnetons, where n is the number of thiolates. In terms of multipole expansion for Monopoles (MDC-m ×, ∘), Dipoles (MDC-d ·, ∇) and Quadrupoles (MDC-q +, ▷).

III. Conclusions

The magnetic moments of $MnAu_6$ and $Mn@Au_{12}$ pure and n-thiolated clusters were calculated using a relativistic DFT-ZORA method. For $Mn@Au_6$, two of the three geometries studied are planar. The non-planar isomer has a C_{2V} symmetry structure and had a high $\boldsymbol{\mu_m}$ of 5 μ_B. Under D_{6h} symmetry, we found four of the seven free electrons of the Mn paired with electrons from gold atoms leaving three unpaired, giving us a magnetic moment of 3 μ_B. However, the most stable structure of the $Mn@Au_6$ isomers had C_S symmetry, and also exhibited the highest value of $\boldsymbol{\mu_m}$ (5 μ_B); also had a large HL-gap (1.03 eV). In all three cases we conclude the jellium model is compatible with our results which explain accurately the resulting $\boldsymbol{\mu_m}$. When we attached thiolates on the D_{6h}, structure in most cases the internal symmetry was conserved, except for the cases of four and five thiolates where plane bending and asymmetric bond elongations become present. With respect to the magnetic moment for three of the six geometries, with 1, 3 and 5 thiolates, the $\boldsymbol{\mu_m}$ is 4 μ_B, clearly not showing change for odd number of thiolates. With even thiolates for $x=2$ the $\boldsymbol{\mu_m}$ is 3 μ_B and for the other two the magnetic moment is 5 μ_B. In all these cases it seems the jellium model fits in adequately and the principal contribution of spin density is provided by the manganese atom. Stable geometries of manganese inside a twelve gold cage-like structure was found for three symmetries, but the icosahedral one was unstable. The structure that was highest in stability and symmetry at equilibrium is the octahedral structure which has a HL-gap of 0.36 eV as well as a high $\boldsymbol{\mu_m}$ of 5 μ_B. The other two symmetries which we identify by C_S and D_{6h} (in terms of their initial structures before relaxation) have a $\boldsymbol{\mu_m}$ values of 5 $\mu_B$and 3 μ_B respectively and HL-gap of 0.18 eV and 0.39 eV. The lowest values of both the HL-gap and $\boldsymbol{\mu_m}$ is seen for the unstable icosahedral structure with 0.08 eV and 1 μ_B. The complexes $Mn@Au_{12}[SCH_3]_n$ (n = 1, 2, 3, 4, 12) were obtained by adding thiolates to $Mn@Au_{12}$ at icosahedral symmetry I_h, and in the process of geometry optimization the cluster was notably distorted, for example with $n=1$ where the symmetry was reduced from icosahedral to octahedral. The contribution of the manganese to the spin density varied between values of 3.16 (~3 μ_B) for $Mn@Au_{12}[SCH_3]_3$ to 4.74 (~5 μ_B) for $Mn@Au_{12}[SCH_3]_4$ according to MPA and 0.36 (~0 μ_B) for $Mn@Au_{12}[SCH_3]_2$ to 4.60 (~5 μ_B) for $Mn@Au_{12}[SCH_3]_{12}$ according to MDC-m.

All the equilibrium isomers exhibit holes exposing the manganese atom in the interior, which could be a characteristic of ferromagnetic elements inside transition metals and a precursor of magnetic gold nanotubes.

Acknowledgements

We would like to thank Prof. T. Wright and J. Harris for fruitful discussions and comments. GR acknowledges the CONACYT Mexico Scholarship for PhD funding (Reg. 215343). We are thankful with the Dirección General de Cómputo y de Tecnologías de la Información y la Comunicación (DGTIC-UNAM) for providing supercomputing resources.

Notes and references

[a] Department of Theoretical and Physical Chemistry, School of Chemistry, University of Nottingham, University Park, Nottingham NG7 2RD, UK. *pcxgr@nottingham.ac.uk

[b] Facultad de Ciencias, Universidad Nacional Autónoma de México, Apdo. Post. 70-646, 04510 México D.F., México. E-mail: jrsoto@unam.mx; Fax: +52 55 5616 0326; Tel: +52 55 5622 4871.

1. P. Pyykkö, *Annu. Rev. Phys. Chem.*, 2012, **63**, 45–64.

2. P. Pyykkö, *Angew. Chem. Int. Ed. Engl.*, 2004, **43**, 4412–56.

3. P. Pyykko, *Chem. Rev.*, 1988, **88**, 563–594.

4. K. Balasubramanian, *Relativistic Effects in Chemistry*, Wiley, New York, 1997.

5. P. Schwerdtfeger and M. Lein, *Gold Chemistry Applications and Future directions in the Life Sciences*, Wiley-VCH, 1st edn., 2009.

6. M. Jansen, *Solid State Sci.*, 2005, **7**, 1464–1474.

7. D. R. McKelvey, *J. Chem. Educ.*, 1983, **60**, 112.

8. M. Samah, M. Bouguerra, L. Guerbous, and M. Berd, *Phys. Scr.*, 2007, **75**, 411–413.

9. A. Deka and R. C. Deka, *J. Mol. Struct. THEOCHEM*, 2008, **870**, 83–93.

10. P. Gruene, D. M. Rayner, B. Redlich, A. F. G. Van Der Meer, J. T. Lyon, G. Meijer, and A. Fielicke, *Science (80-.).*, 2008, **321**, 674–676.

11. B. Assadollahzadeh and P. Schwerdtfeger, *J. Chem. Phys.*, 2009, **131**, 064306.

12. D. Dong, K. Xiao-Yu, G. Jian-Jun, and Z. Ben-Xia, *J. Phys. Chem. Solids*, 2010, **71**, 770–775.

13. B. Simard and P. A. Hackett, *J. Mol. Spectrosc.*, 1990, **142**, 310–318.

14. J. Ho, K. M. Ervin, and W. C. Lineberger, *J. Chem. Phys.*, 1990, **93**, 6987–7002.

15. M. Zhang, L. He, L. Zhao, X. Feng, and Y. Luo, *J. Phys. Chem. C*, 2009, **113**, 6491–6496.

16. P. Schwerdtfeger, *Angew. Chem. Int. Ed. Engl.*, 2003, **42**, 1892–5.

17. E. Janssens, H. Tanaka, S. Neukermans, R. E. Silverans, and P. Lievens, *New J. Phys.*, 2003, **5**, 46–46.

18. X. Li, B. Kiran, L.-F. Cui, and L.-S. Wang, *Phys. Rev. Lett.*, 2005, **95**, 253401.

19. U. Rohrmann and R. Schäfer, *Phys. Rev. Lett.*, 2013, **111**, 133401.

20. M. Zhang, S. Chen, Q. M. Deng, L. M. He, L. N. Zhao, and Y. H. Luo, *Eur. Phys. J. D*, 2010, **58**, 117–123.

21. F. Schiller and C. Laubschat, *J. Magn. Magn. Mater.*, 2004, **272-276**, E239–E240.

22. T. Höltzl, P. Lievens, T. Veszprémi, and M. T. Nguyen, *J. Phys. Chem. C*, 2009, **113**, 21016–21018.

23. R. Masrour, E. K. Hlil, M. Hamedoun, a. Benyoussef, O. Mounkachi, and L. Bahmad, *J. Magn. Magn. Mater.*, 2013, **326**, 166–170.

24. J. Wang, J. Bai, J. Jellinek, and X. C. Zeng, *J. Am. Chem. Soc.*, 2007, **129**, 4110–1.

25. M. Zhou, Y. Q. Cai, M. G. Zeng, C. Zhang, and Y. P. Feng, *Appl. Phys. Lett.*, 2011, **98**, 143103.

26. a Ayuela, P. Crespo, M. a García, A. Hernando, and P. M. Echenique, *Arxiv Prepr. arXiv11014109*, 2011, **14**, 1–13.

27. J. Akola, M. Walter, R. L. Whetten, H. Häkkinen, and H. Grönbeck, *J. Am. Chem. Soc.*, 2008, **130**, 3756–7.

28. T. Iwasa and K. Nobusada, *Chem. Phys. Lett.*, 2007, **441**, 268–272.

29. A. C. Templeton, W. P. Wuelfing, and R. W. Murray, *Acc. Chem. Res.*, 2000, **33**, 27–36.

30. M. Daniel and D. Astruc, *Chem. Rev.*, 2004, **104**, 293–346.

31. X. Chen, M. Strange, and H. Häkkinen, *Phys. Rev. B*, 2012, **85**, 085422.

32. Y. Negishi, K. Nobusada, and T. Tsukuda, *J. Am. Chem. Soc.*, 2005, **127**, 5261–70.

33. Y. Negishi, H. Tsunoyama, M. Suzuki, N. Kawamura, M. M. Matsushita, K. Maruyama, T. Sugawara, T. Yokoyama, and T. Tsukuda, *J. Am. Chem. Soc.*, 2006, **128**, 12034–5.

34. M. Zhu, C. M. Aikens, F. J. Hollander, G. C. Schatz, and R. Jin, *J. Am. Chem. Soc.*, 2008, **130**, 5883–5.

35. F. Jensen, *J. Chem. Theory Comput.*, 2008, **4**, 719–727.

36. Y. Shichibu, Y. Negishi, H. Tsunoyama, M. Kanehara, T. Teranishi, and T. Tsukuda, *Small*, 2007, **3**, 835–9.

37. O. Lopez-Acevedo, H. Tsunoyama, T. Tsukuda, H. Häkkinen, and C. M. Aikens, *J. Am. Chem. Soc.*, 2010, **132**, 8210–8.

38. G. Te Velde, F. M. Bickelhaupt, E. J. Baerends, C. Fonseca Guerra, S. J. a Van Gisbergen, J. G. Snijders, and T. Ziegler, *J. Comput. Chem.*, 2001, **22**, 931–967.

39. W. Kohn and L. J. Sham, *Phys. Rev.*, 1965, **140**, A1133–A1138.

40. J. P. Perdew and Y. Wang, *Phys. Rev. B*, 1992, **45**, 244–249.

41. E. Van Lenthe, A. Ehlers, and E.-J. Baerends, *J. Chem. Phys.*, 1999, **110**, 8943–8953.

42. R. S. Mulliken, *J. Chem. Phys.*, 1955, **23**, 1833.

43. M. Swart, P. T. van Duijnen, and J. G. Snijders, *J. Comput. Chem.*, 2001, **22**, 79–88.

44. L. Zhu, J. Wang, and F. Ding, *J. Chem. Phys.*, 2009, **130**, 064706.